The contributions of respiration and glycolysis to extracellular acid production

Shona A. Mookerjee [a,b,*], Renata L.S. Goncalves [b], Akos A. Gerencser [a,b], David G. Nicholls [b], Martin D. Brand [a,b]

[a] College of Pharmacy, Touro University California, 1310 Club Drive, Vallejo, CA 94592, USA
[b] Buck Institute for Research on Aging, 8001 Redwood Blvd, Novato, CA 94945, USA

ARTICLE INFO

ABSTRACT

Background: The rate at which cells acidify the extracellular medium is frequently used to report glycolytic rate, with the implicit assumption that conversion of uncharged glucose or glycogen to lactate$^-$ + H$^+$ is the only significant source of acidification. However, another potential source of extracellular protons is the production of CO_2 during substrate oxidation: CO_2 is hydrated to H_2CO_3, which then dissociates to HCO_3^- + H$^+$.
Methods: O$_2$ consumption and pH were monitored in a popular platform for measuring extracellular acidification (the Seahorse XF Analyzer).
Results: We found that CO_2 produced during respiration caused almost stoichiometric release of H$^+$ into the medium. With C2C12 myoblasts given glucose, respiration-derived CO_2 contributed 34% of the total extracellular acidification. When glucose was omitted or replaced by palmitate or pyruvate, this value was 67–100%. Analysis of primary cells, cancer cell lines, stem cell lines, and isolated synaptosomes revealed contributions of CO_2-produced acidification that were usually substantial, ranging from 3% to 100% of the total acidification rate.
Conclusion: Measurement of glycolytic rate using extracellular acidification requires differentiation between respiratory and glycolytic acid production.
General significance: The data presented here demonstrate the importance of this correction when extracellular acidification is used for quantitative measurement of glycolytic flux to lactate. We describe a simple way to correct the measured extracellular acidification rate for respiratory acid production, using simultaneous measurement of oxygen consumption rate.
Summary statement: Extracellular acidification is often assumed to result solely from glycolytic lactate production, but respiratory CO_2 also contributes. We demonstrate that extracellular acidification by myoblasts given glucose is 66% glycolytic and 34% respiratory and describe a method to differentiate these sources.

1. Introduction

Assessing metabolic flux is essential to understanding cellular metabolism, and the measurement of oxygen consumption and extracellular acidification by adherent cells is now routine using instruments such as the Seahorse XF Analyzer [1–4]. The rate of mitochondrial oxygen consumption is reliably calculated as total cellular oxygen consumption rate minus any oxygen consumption that is insensitive to specific inhibitors of mitochondrial electron transport [5–7]. In small wells in polystyrene plates, the oxygen diffusion between the wells, the polystyrene, and the atmosphere is considerable and must be accounted for [4].

With these constraints, oxygen consumption rate is a direct and quantitative measure of mitochondrial electron transport rate.

Extracellular acidification is an equally accessible measurement of metabolic activity. A major component of extracellular acidification is the glycolytic production of lactate [8]. At physiological pH around 7, glucose is uncharged, whereas lactate (pK_a 3.86) exists primarily as the carboxylate anion. Net conversion of glucose to lactate$^-$ at neutral pH necessarily releases protons and acidifies the medium, so extracellular acidification rate is commonly used as a direct and quantitative measure of glycolytic rate [1,2,8–11]. However, the relationship between extracellular acidification and glycolytic rate is confounded by other acidification mechanisms. Specifically, CO_2 generated in the tricarboxylic acid cycle can be spontaneously or enzymatically hydrated to carbonic acid, H_2CO_3, which dissociates to HCO_3^- + H$^+$ in aqueous media at physiological pH. Conversion of one glucose molecule to lactate yields 2 lactate$^-$ + 2 H$^+$, whereas complete oxidation of one glucose to CO_2 yields 6 HCO_3^- + 6 H$^+$, so the extracellular acidification when a glucose molecule is oxidized to CO_2 is three times greater than the extracellular acidification when it is converted to lactate.

Here, we show that CO_2 produced by respiration in the wells of a polystyrene multiwell plate is completely retained in the wells, causing almost stoichiometric acidification. The acidification can be calculated from the rate of respiration, the respiratory quotient, the net H^+ production per CO_2 generated, and the pH buffering power of the medium. Analysis of extracellular acidification by C2C12 myoblasts reveals that CO_2 production accounts for most or all of the extracellular acidification by cells given no substrate or with added pyruvate or palmitate, and 34% of the total extracellular acidification by cells oxidizing added glucose. In other cell lines, CO_2 also contributes substantially to extracellular acidification, even in many of those reported to be highly glycolytic.

2. Materials and methods

2.1. Reagents

Chemicals were from Sigma. Cell culture reagents and consumables were from Corning. Seahorse XF consumables were from Seahorse Bioscience.

2.2. Mitochondria

Rat skeletal muscle mitochondria were isolated according to [12]. Rats were used in accordance with IACUC standards under a protocol approved by the Buck Institute Animal Care and Use Committee. Rates of oxygen consumption and acidification were measured using a Seahorse XF24 Extracellular Flux Analyzer (Seahorse Bioscience) [13] in MAS-1 medium (2 mM HEPES, 10 mM KH_2PO_4, 1 mM EGTA, 70 mM sucrose, 220 mM mannitol, 5 mM $MgCl_2$, 0.2% fatty-acid-free bovine serum albumin (Sigma A3803)) containing 4 µM carbonylcyanide 4-(trifluoromethoxy)-phenylhydrazone (FCCP), 2.5 µg/mL oligomycin, 5 mM dichloroacetate, 5 mM aminooxyacetate, 5 mM fluoroacetate, and 2 µM atpenin A5. Oxygen consumption was corrected for rotenone-insensitive rates. Extramitochondrial acidification rate was corrected for background by subtraction of rates in sample-free wells.

2.3. Cells

Mouse C2C12 myoblasts [14] were cultured in Dulbecco's modified Eagle medium (DMEM) with 11.1 mM glucose, 2 mM glutamine, 10% v/v fetal bovine serum (FBS), 100 U/mL penicillin, and 100 µg/mL streptomycin. Twenty-four hours prior to assay, cells were plated in 100 µL culture medium at 20,000 cells/well in a 24-well polystyrene V7-PS Flux plate with no additional coating. 25 min prior to assay, cells were washed three times with and then incubated in a final volume of 500 µL Krebs–Ringer phosphate HEPES (KRPH) medium (2 mM HEPES, 136 mM NaCl, 2 mM NaH_2PO_4, 3.7 mM KCl, 1 mM $MgCl_2$, 1.5 mM $CaCl_2$, 0.1% w/v fatty-acid-free bovine serum albumin, pH 7.4 at 37 °C). At assay start, medium was replaced with fresh KRPH containing 500 U/mL carbonic anhydrase (Sigma C2624) and either pyruvate (10 mM), glucose (10 mM), carnitine and palmitate (0.5 mM each), or no substrate. Cell respiratory control was assayed by stepwise addition of A: 2 µg/mL oligomycin; B: 0.5 µM FCCP; C: 1 µM rotenone, 1 µM myxothiazol, 5 mM 2-deoxyglucose; D: HCl. Two measurement cycles of 2 min mix, 1 min wait, and 5 min measure were carried out after each addition, with three cycles following the final addition. Following the assay, samples were removed for lactate analysis, and wells were washed three times with 250 µL BSA-free KRPH. Twenty-five microliters of RIPA lysis buffer (150 mM NaCl, 50 mM Tris, 1 mM EGTA, 1 mM EDTA, 1% v/v Triton X-100, 0.5% w/v sodium deoxycholate, 0.1% v/v SDS, pH 7.4 at 22 °C) was added. Cells were incubated on ice for 30 min and agitated on a plate shaker at 1200 rpm for 5 min. Protein concentration was measured by BCA assay. Protein content was ~4 µg/well.

ZR75 mammary ductal carcinoma [15] and SJSA-1 osteosarcoma [16] cells were cultured in RPMI 1640 with 10% v/v FBS; MCF7 mammary adenocarcinoma cells [17] were cultured in low-glucose (5.5 mM) DMEM with 10% v/v FBS. All lines were assayed in a minimal TES buffer containing 3.5 mM KCl, 120 mM NaCl, 1.3 mM $CaCl_2$, 0.4 mM KH_2PO_4, 1.2 mM Na_2SO_4, 2 mM $MgCl_2$, 15 mM glucose, 20 mM TES, and 0.3% w/v BSA at pH 7.4 at 37 °C. I6 embryonic stem cells and neural stem cells were cultured and assayed as described [18]. Primary rat cortical neurons prepared as in [19] were assayed in minimal TES as above modified with 1 mM $MgCl_2$ and 0.4% w/v BSA. Dispersed rat islets prepared as in [20] were assayed in RPMI medium devoid of phenol red, riboflavin and folic acid, containing 3 mM glucose, 2 mM glutamine, 5 mM $NaHCO_3$, 1.5 mM $CaCl_2$, 1 mM $MgCl_2$, 20 mM TES, and 1% v/v FBS, pH 7.4 at 37 °C. INS1E pancreatic insulinoma cells [21] were cultured in RPMI 1640 with 11 mM glucose, 10% v/v FBS, 10 mM HEPES, 2 mM glutamine, 50 µM β-mercaptoethanol, 100 U/mL penicillin, 100 µg/mL streptomycin at 37 °C, 5% CO_2, and assayed in minimal TES as above modified with 1 mM $MgCl_2$, 0.5 mM KH_2PO_4, 5 mM $NaHCO_3$, 10 mM Na-TES, 2 mM glucose, and 2 mM glutamine. Mouse cortical synaptosomes were isolated and assayed as in [22].
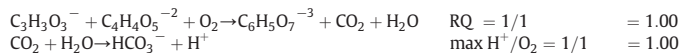
2.4. Lactate measurement

End point lactate concentration was determined in a 96-well plate by measuring the initial velocity (2 min) of $NAD^+ \rightarrow NADH$ by lactate dehydrogenase. Immediately following the extracellular flux assay, 100 µL of assay medium was diluted 1:1 with 2× hydrazine buffer (1× composition 500 mM Tris, 10 mM EDTA, 200 mM hydrazine, 2 mM NAD^+, 20 U/mL lactate dehydrogenase, pH 9.8 at 22 °C). NADH fluorescence at 340 nm excitation/460 nm emission was monitored in a BMG Pherastar FS microplate reader and calibrated against known lactate concentrations from 0 to 50 µM. Lactate in glucose-containing wells was ~40 µM.

2.5. Calculations

The respiratory quotient (RQ; CO_2 produced/O_2 consumed) for complete or partial oxidation of a substrate is reaction pathway-independent and can be calculated from the relevant balanced equation. Similarly, the maximum H^+ released per O_2 consumed by respiration can be calculated (if all of the CO_2 generates HCO_3^- in the well, see Results):
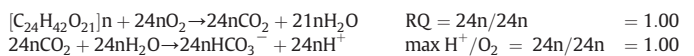
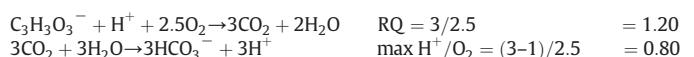For conversion of pyruvate$^-$ plus malate^{-2} entirely to citrate^{-3} (Fig. 1A):

$$C_3H_3O_3{}^- + C_4H_4O_5{}^{-2} + O_2 \rightarrow C_6H_5O_7{}^{-3} + CO_2 + H_2O \qquad RQ = 1/1 \qquad = 1.00$$
$$CO_2 + H_2O \rightarrow HCO_3{}^- + H^+ \qquad\qquad\qquad max\ H^+/O_2 = 1/1 \qquad = 1.00$$

For complete oxidation of glucose

$$C_6H_{12}O_6 + 6O_2 \rightarrow 6CO_2 + 6H_2O \qquad RQ = 6/6 \qquad\qquad = 1.00$$
$$6CO_2 + 6H_2O \rightarrow 6HCO_3{}^- + 6H^+ \qquad max\ H^+/O_2 = 6/6 \qquad = 1.00$$

For complete oxidation of glycogen

$$[C_{24}H_{42}O_{21}]n + 24nO_2 \rightarrow 24nCO_2 + 21nH_2O \qquad RQ = 24n/24n \qquad\qquad = 1.00$$
$$24nCO_2 + 24nH_2O \rightarrow 24nHCO_3{}^- + 24nH^+ \qquad max\ H^+/O_2 = 24n/24n \qquad = 1.00$$

For complete oxidation of pyruvate$^-$

$$C_3H_3O_3{}^- + H^+ + 2.5O_2 \rightarrow 3CO_2 + 2H_2O \qquad RQ = 3/2.5 \qquad\qquad = 1.20$$
$$3CO_2 + 3H_2O \rightarrow 3HCO_3{}^- + 3H^+ \qquad max\ H^+/O_2 = (3-1)/2.5 \qquad = 0.80$$

For complete oxidation of palmitate$^-$

$$C_{16}H_{31}O_2{}^- + H^+ + 23O_2 \rightarrow 16CO_2 + 16H_2O \qquad RQ = 16/23 \qquad\qquad = 0.70$$
$$16CO_2 + 16H_2O \rightarrow 16HCO_3{}^- + 16H^+ \qquad max\ H^+/O_2 = (16-1)/23 \qquad = 0.65$$

For complete oxidation of glutamine

$$C_5H_{10}N_2O_3 + 4.5O_2 \rightarrow 5CO_2 + 2H_2O + 2NH_3 \qquad RQ = 5/4.5 \qquad = 1.11$$
$$5CO_2 + 2NH_3 + 5H_2O \rightarrow 5HCO_3^- + 2NH_4^+ + 3H^+ \qquad max\ H^+/O_2 = 3/4.5 \qquad = 0.67$$
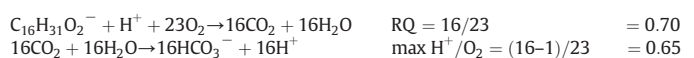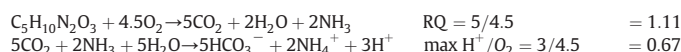
Some dissolved CO_2 (~5% at pH 7.4) is not hydrated at equilibrium. Net H^+/O_2 is calculated as max H^+/O_2 multiplied by the fraction of CO_2 converted, $HCO_3^-/(CO_2 + HCO_3^-) = 10^{(pH-pK_1)}/(1 + 10^{(pH-pK_1)}$, where pK_1 is the overall pK for $CO_{2(aq)} + H_2O \rightarrow HCO_3^- + H^+ = 6.093$ at 37 °C [23, p. 45].

3. Results

3.1. CO$_2$ produced in a polystyrene multiwell plate causes almost stoichiometric acidification

We established and validated a convenient model system to quantify the rate of CO_2 generation in individual wells of a polystyrene Seahorse 24-well plate then used it to determine what proportion of the generated CO_2 was retained in the well, hydrated to H_2CO_3, and dissociated to form HCO_3^- and H^+ to acidify the medium.
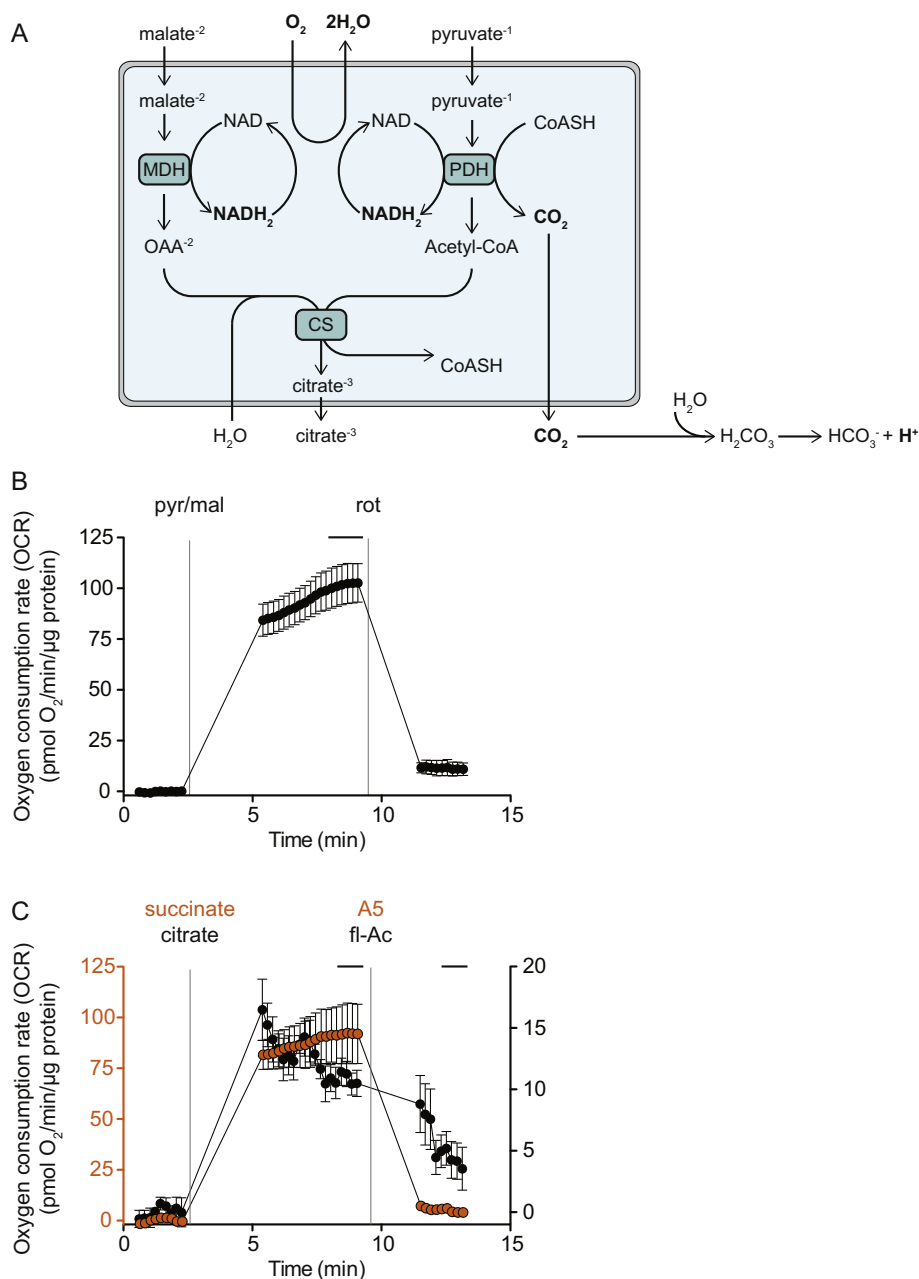

Fig. 1. Reactions of the model CO_2-generating system. (A) Metabolic reactions involved in CO_2 generation by isolated rat skeletal muscle mitochondria respiring on pyruvate plus malate and generating citrate. MDH, malate dehydrogenase; PDH, pyruvate dehydrogenase; CS, citrate synthase. (B) Oxygen consumption rate of mitochondria in the presence of 4 μM FCCP, 2.5 μg/mL oligomycin, 5 mM dichloroacetate, 5 mM aminooxyacetate, 5 mM fluoroacetate, and 2 μM atpenin A5 measured in the Seahorse XF24. 10 mM pyruvate plus 2 mM malate and 1 μM rotenone were added as indicated. Data are means ± SEM of $n = 6$ independent biological replicates. (C) Efficacy of fluoroacetate and atpenin A5. Respiration caused by addition of citrate (black axis and symbols) or succinate (red axis and symbols) was inhibited by subsequent addition of fluoroacetate or atpenin A5, respectively. Data are means ± SEM of $n = 3$ independent biological replicates. Horizontal bars: the mean of this range was used for subsequent calculations.

3.1.1. Model CO_2-generating system with known RQ

To generate CO_2 at a rate that could be measured easily and accurately, we used isolated skeletal muscle mitochondria running defined metabolic reactions (Fig. 1A). Addition of pyruvate plus malate initiated the following overall reaction:

$$Pyruvate^- + malate^{-2} + O_2 \rightarrow citrate^{-3} + H_2O + CO_2$$
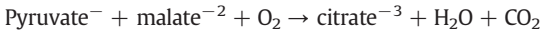
Oxidation of one pyruvate yields one CO_2 and one NADH + H$^+$ (shown as $NADH_2$). Oxidation of malate yields a second $NADH_2$. The 4 e$^-$ donated to electron transport reduce one O_2 to $2H_2O$. RQ is therefore 1, and the rate of CO_2 production exactly equals the rate of O_2 consumption.

This system was pharmacologically constrained to the reactions in Fig. 1A. To maximize the measured rates, dichloroacetate was added to activate pyruvate dehydrogenase. Mitochondria were uncoupled using FCCP to ensure no limitation by respiratory control. ATP synthesis was inhibited by uncoupling and by adding oligomycin. Metabolism of pyruvate or oxaloacetate by aminotransferases was inhibited by adding aminooxyacetate. Metabolism of endogenous substrates in the tricarboxylic acid cycle upstream of malate was restricted by adding atpenin A5 to inhibit succinate dehydrogenase. Metabolism downstream of citrate was limited by adding fluoroacetate to inhibit aconitase. FCCP also inhibits conversion of pyruvate to oxaloacetate by pyruvate carboxylase, by preventing ATP production.

Fig. 1B shows that oxygen consumption by this model system was initially negligible (therefore no endogenous substrates contributed significantly to respiration). After addition of pyruvate plus malate, oxygen consumption reached a high, stable rate that was strongly inhibited by rotenone.

Separate experiments confirmed that succinate dehydrogenase and aconitase were inhibited under our conditions. Fig. 1C shows that atpenin A5 fully inhibited succinate oxidation and fluoroacetate substantially decreased citrate oxidation. These controls confirm the accuracy of Fig. 1A and therefore that CO_2 production rate is equal to O_2 consumption rate in this model system.

3.1.2. CO_2 production causes almost stoichiometric acidification

Having established the model system to generate CO_2 at measurable rates with an unambiguous RQ of 1.0 (Fig. 1), we used it to determine the proportion of the generated CO_2 that was retained in the well and led to extracellular acidification.

Fig. 2A shows the pH measured simultaneously with the oxygen consumption in Fig. 1B. Acidification of the medium was initially negligible (therefore no endogenous substrates or reactions contributed significantly to acidification). After addition of pyruvate plus malate, acidification reached a high, stable rate. This rate was caused by the hydration of CO_2 to produce H_2CO_3 and then $HCO_3^- + H^+$ as in Fig. 1A, and as expected was strongly inhibited by rotenone.

In control experiments, we compared the acidification rate in the presence and absence of added carbonic anhydrase (up to 500 U/mL) and found no difference. Similarly, oxygen consumption rate was not different (data not shown), showing either the presence of sufficient endogenous carbonic anhydrase in our crude mitochondrial preparations or a sufficient rate of spontaneous CO_2 hydration. Therefore, it was unnecessary to make routine additions of carbonic anhydrase to this model system.

To enable conversion of the measured acidification rate from mpH units/min/μg protein to pmol H$^+$/min/μg protein, we measured the buffering power of the medium. We added different known amounts of HCl after each experiment and recorded the change in pH from pre-addition to 5 min after addition (Fig. 2B, horizontal bars). Fig. 2C shows that pH responded pseudo-linearly to H$^+$ in the measuring volume over the small pH range monitored in Fig. 2A. Linear regression gave a slope (buffering power) of −0.018 mpH/pmol H$^+$ in MAS-1 medium. The value was confirmed by recording the changes in pH caused by adding known amounts of HCl to bulk samples of the medium using a pH meter. Using this value we calculated the proton production rates (Fig. 2D).

To determine how much of the respiratory CO_2 remained in the wells as HCO_3^-, we compared the measured acidification rate with the rate of CO_2 production calculated from the rotenone-sensitive oxygen consumption rate (Fig. 3). If the CO_2 all remained in the assay medium
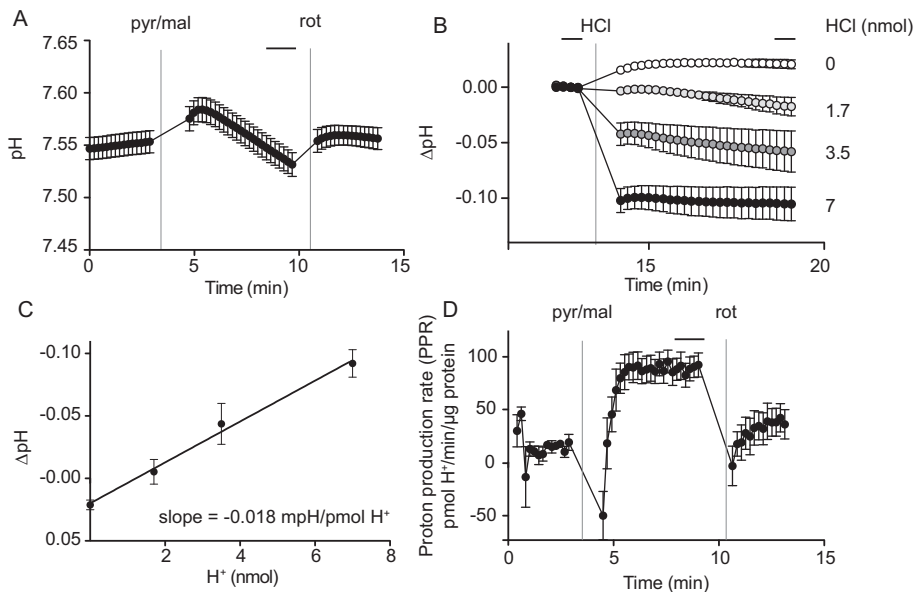

Fig. 2. Changes in pH and proton production rate caused by CO_2 production in the model system. (A) pH of the medium measured in the same experiments as Fig. 1B. Horizontal bar: pH values used to calculate acidification rate. (B) Acid calibration of buffering power. Different amounts of HCl were added from port C where indicated, in continuations of the experiment in A. Data were normalized to the mean of the last three points measured before acid addition. Values for HCl added are given relative to the 7 μL measuring volume, i.e., 1 mM added HCl corresponded to 7 nmol HCl in the measuring volume. Horizontal bars indicate initial and final data used to calculate the changes in pH. (C) Change in pH as a function of H$^+$ added to the 7 μL measuring volume (data from B). The slope is the buffering power, used to calibrate the rates of pH change shown in (A). (D) Proton production rate (PPR) calculated using the pH trace (A), calibration (B, C) and mitochondrial protein loaded per well. Horizontal bar: values used for proton production rate in Fig. 3. Data are means ± SEM of $n = 6$ independent biological replicates.
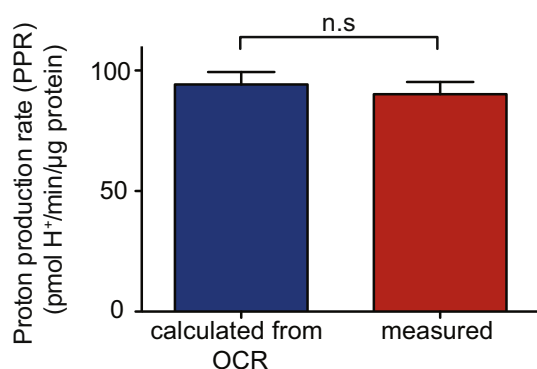
Fig. 3. Proton production rates calculated from oxygen consumption rate and measured using calibrated pH changes. The calculated proton production rate was determined from the rotenone-sensitive oxygen consumption rate in Fig. 1B (see Materials and Methods). The measured proton production rate was taken from Fig. 2D. Data are means $\pm$ SEM of $n = 6$ independent biological replicates. n.s.: $p = 0.58$, two-tailed paired Student's t-test.

as HCO_3^-, the measured proton production rate would exactly equal the rate calculated using the oxygen consumption rate. If some CO_2 diffused into the polystyrene or the atmosphere or was lost in some other way, the measured rate would be proportionately less than the rate calculated from oxygen consumption. This design enabled quantitative calculation of any potential CO_2 loss from the wells. The rate calculated from oxygen consumption after correction for unhydrated CO_2 was 94.3 ± 5.1 pmol H^+/min/µg protein ($n = 6$), whereas the rate measured by extracellular acidification was 90.2 ± 5.1 pmol H^+/min/µg protein ($n = 6$), which is $96\% \pm 7\%$ of the rate calculated from oxygen consumption. The measured and calculated values were not significantly different. These experiments show that essentially all CO_2 generated by respiration in the wells of a Seahorse V7-PS Flux plate remains in the wells as HCO_3^- and causes almost stoichiometric acidification of the medium. The rate of acidification caused by CO_2 production can therefore be quantitatively determined from the oxygen consumption rate if the overall metabolic reaction is known.

3.2. Sources of extracellular acidification by cells

3.2.1. Theoretical considerations

Fig. 4A shows the pathways expected to cause extracellular acidification with different substrates in cells. The overall reactions, RQs, and max H^+/O_2 values are given in Materials and Methods.

When extracellular glucose (or endogenous glycogen) is used, it forms pyruvate$^-$ + H^+. The pyruvate has two possible major fates. It may complete anaerobic glycolysis and generate lactate through lactate dehydrogenase (using the NADH generated by glyceraldehyde 3-phosphate dehydrogenase), followed by export with H^+ to the medium. The total extracellular acidification will be 1 H^+ per lactate produced (and pyruvate consumed). Alternatively, it may enter the tricarboxylic acid cycle where, if the pyruvate is fully oxidized, 1 H^+ will be consumed and 3 CO_2 will be released, one each at pyruvate dehydrogenase, isocitrate dehydrogenase, and 2-oxoglutarate dehydrogenase. The total extracellular acidification from this pathway will be 3 H^+ per pyruvate oxidized; 1 H^+ per CO_2 generated. Since the RQ for complete oxidation of glucose or glycogen is 1.0 (see Materials and Methods), a maximum of 1.0 H^+ will be generated per O_2 consumed by the mitochondria.

When extracellular pyruvate is used, cells take up pyruvate$^-$ + H^+ [24]. Conversion to lactate will cause no net acidification of the extracellular medium and will be very limited by rapid depletion of cytosolic NADH. Instead, most of the pyruvate will be oxidized in the mitochondria as above. In this case, the total extracellular acidification will be

2 H^+ per pyruvate oxidized (3 H^+ produced from H_2CO_3 and 1 H^+ consumed during pyruvate catabolism); $^2/_3$ H^+ per CO_2 generated. Since the RQ for complete oxidation of pyruvate is 1.2 (see Materials and Methods), respiration on pyruvate will generate a maximum of $^2/_3 \times 1.2 = 0.8$ H^+ per O_2 consumed.

When extracellular palmitate is used, cells will take up palmitate$^-$ + H^+ and generate palmitoyl-CoA [25]. This will enter the mitochondria through the carnitine shuttle and, if fully oxidized, generate 16 CO_2. The total acidification will be 15 H^+ per palmitate oxidized (16 H^+ produced from CO_2 and 1 H^+ consumed at palmitoyl CoA synthase). Overall, since the RQ for complete oxidation of palmitate is 0.7 (see Materials and Methods), respiration on palmitate will generate a maximum of $^{15}/_{16} \times 0.7 = 0.65$ H^+ per O_2 consumed.

Complete oxidation of glutamine will yield 5 CO_2 and consume 4.5 O_2. The total acidification will be 3 H^+ per glutamine oxidized; 5 H^+ produced from CO_2 and 2 H^+ consumed by conversion of NH_3 to NH_4^+ (see Materials and Methods), so respiration on glutamine will generate a maximum of $^3/_{4.5} = 0.67$ H^+ per O_2 consumed

In the absence of added substrate, cells will metabolize endogenous substrates, and we assume a respiratory quotient of 1.0, based on mixed substrate usage (glycogen, proteins and fats), and a maximum of 1.0 H^+ per O_2 consumed.

Because essentially all the CO_2 remains in the well (Fig. 3), the acidification caused by HCO_3^- + H^+ production can be calculated from the mitochondrial oxygen consumption rate (OCR) multiplied by the maximum H^+/O_2 (1.0 for glucose and glycogen, 0.8 for pyruvate, 0.65 for palmitate, see Calculations) and by the fraction of CO_2 that is converted to HCO_3^- + H^+ at the experimental temperature and pH. Glycolytic rate is therefore the proton production rate (PPR) remaining after subtraction of the PPR caused by CO_2 production, where PPR is the extracellular acidification rate (ECAR) expressed in pmol H^+/min/µg protein (requiring calibration of the pH buffering power of the medium), OCR is in pmol O_2/min/µg protein, and lactate production rate and glycolytic rate are in pmol lactate/min/µg protein. Thus:

$$\text{Glycolytic rate} = \text{PPR}_g = \text{PPR}_{tot} - \text{PPR}_{resp} \tag{1}$$

where the glycolytic proton production rate (PPR_g) equals the total PPR (PPR_{tot}) minus respiratory PPR (PPR_{resp}). The experimental inputs are revealed in the expanded equation:

$$\text{Glycolytic rate} = (\text{ECAR}_{tot}/\text{BP}) - \left(\text{OCR}_{tot} - \text{OCR}_{rot/myx}\right)\left(\text{max } H^+/O_2\right) \\ \times (\text{HCO}_3^- / (\text{CO}_2 + \text{HCO}_3^-)) \tag{2}$$

where ECAR = extracellular acidification rate (mpH/min), BP = buffering power (mpH/pmol H^+), OCR = oxygen consumption rate (pmol O_2/min), and $\text{OCR}_{rot/myx}$ = non-mitochondrial OCR remaining after complete mitochondrial inhibition. The term describing the fraction of CO_2 that generates HCO_3^- + H^+ can be further expanded to include experimental input:

$$\text{Glycolytic rate} = (\text{ECAR}_{tot}/\text{BP}) - \left(\text{OCR}_{tot} - \text{OCR}_{rot/myx}\right)\left(\text{max } H^+/O_2\right) \\ \times \left(10^{\text{pH}-\text{pK}_1} / \left(1 + 10^{\text{pH}-\text{pK}_1}\right)\right) \tag{3}$$

where K_1 is the combined equilibrium constant of CO_2 hydration and H_2CO_3 dissociation to HCO_3^- + H^+, i.e., the overall pK for $CO_{2(aq)}$ + $H_2O \rightarrow HCO_3^-$ + H^+ = 6.093 at 37 °C [23], p. 45.

3.2.2. Respiratory acidification contributes substantially to total extracellular acidification

We used C2C12 myoblasts to determine the respiratory (CO_2-derived) extracellular acidification when both glycolysis and respiration were potentially active. Myoblasts are common models for investigating metabolism and are readily assayed in the Seahorse [2,26–28].
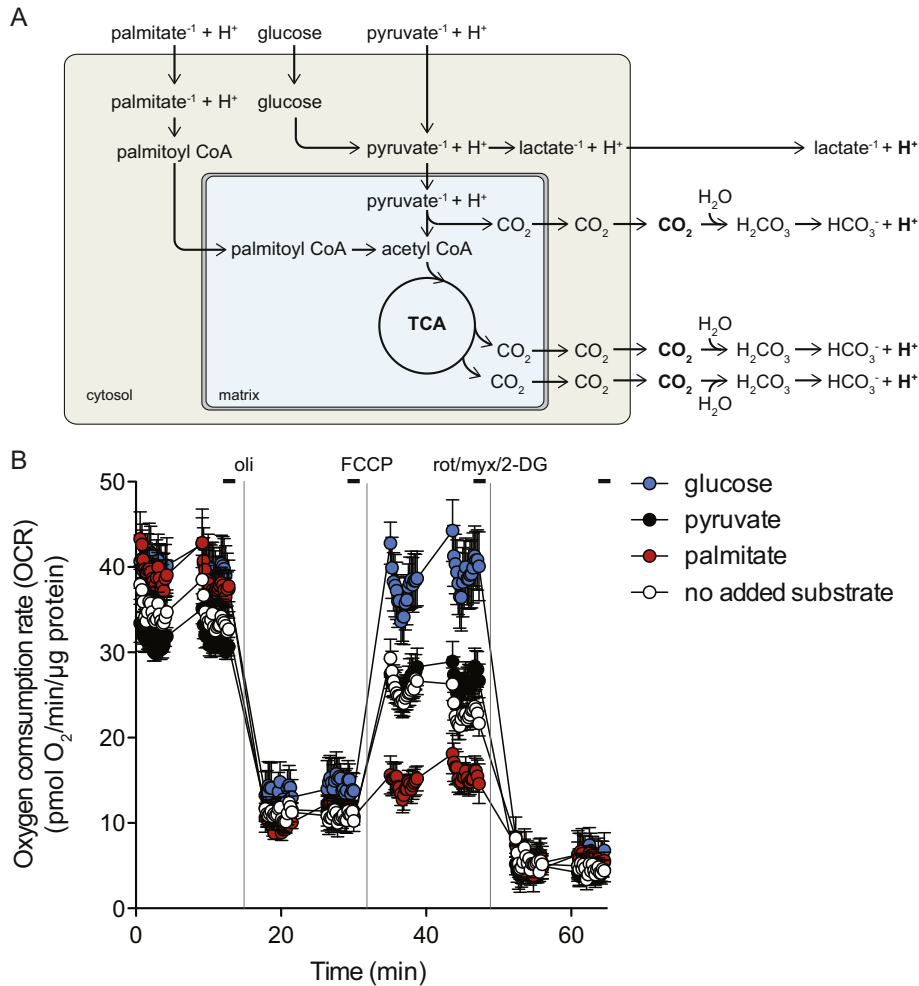
Fig. 4. Cellular catabolism causing oxygen consumption and extracellular acidification. (A) Catabolism of substrates that feed into glycolysis or the tricarboxylic acid cycle (TCA). Reoxidation of intramitochondrial NADH and FADH generated by redox shuttles, β-oxidation and tricarboxylic acid cycle flux causes oxygen consumption by the electron transport chain (not shown). Pathways leading to extracellular acidification caused by production of lactate and CO_2 are drawn explicitly. (B) Oxygen consumption rate of C2C12 cells during standard measurement of cell respiratory control in the Seahorse XF-24 with different substrates (10 mM glucose, 10 mM pyruvate, 0.5 mM palmitate in 1% w/v BSA plus 0.5 mM carnitine, or no added substrate). 2 μg/mL oligomycin (oli); 0.5 μM FCCP, and 1 μM rotenone (rot) plus 1 μM myxothiazol (myx) plus 5 mM 2-deoxyglucose (2-DG) were added as indicated. Horizontal bars: OCR values used for calculations of CO_2-dependent extracellular acidification. Data are means ± SEM of $n = 8$ independent biological replicates. Note that FCCP concentrations were not re-optimized to capture maximal respiratory capacity, as capacity was not the measurement of interest here.

The rate of O_2 consumption and the pH were measured in the presence of three different single substrates with known RQ values: glucose, pyruvate, and palmitate, and also with no added substrate. We were primarily interested in the initial "native" conditions with substrate present and inhibitors absent, but we also performed a conventional cell respiratory control assay [5].

Although carbonic anhydrase was not required in the mitochondrial model system to fully convert CO_2 to $HCO_3^- + H^+$, pilot experiments with C2C12 cells indicated that the presence of carbonic anhydrase increased acidification rates 1.1- to 1.2-fold (not shown). We therefore added carbonic anhydrase to all C2C12 myoblast assays (see Materials and Methods) to ensure complete conversion.

Fig. 4B shows the oxygen consumption rates for this system. Native (baseline) rates were similar with all substrates at 30–40 pmol O_2/μg protein. The cell respiratory control assay allows the determination of the sources of respiratory demand on the cell by ATP turnover and by mitochondrial proton leak (as distinguished by oligomycin) as well as the respiration rate when cells are fully uncoupled (with FCCP). Finally, non-mitochondrial respiration was measured by addition of the electron transport inhibitors rotenone and myxothiazol. To slow glycolytic rate at the end of the experiment, we also added

the glycolysis inhibitor 2-deoxyglucose. Non-mitochondrial rates and the proportion of native rate used to drive ATP synthesis and proton leak were generally similar with all substrates tested, but the uncoupled rates were lower with no added substrate or with added pyruvate or palmitate.

Fig. 5 shows the corresponding pH measurements and calibration of buffering power conducted by port additions of known amounts of HCl in separate wells. pH responded pseudo-linearly to H^+ in the measuring volume over the small pH range monitored. Linear regression gave a buffering power of -0.045 mpH/pmol H^+ in KRPH medium. Fig. 5C shows the acidification rates derived from the data in Fig. 5A, expressed as extracellular acidification rate (ECAR) in units of mpH/min/μg protein and as proton production rate (PPR) after calibration using the slope from Fig. 5B, in units of pmol H^+/min/μg protein. Acidification was rapid with glucose as substrate, increased as expected when mitochondrial ATP synthesis was inhibited by oligomycin and decreased as expected when respiratory CO_2 production was stopped by addition of rotenone plus antimycin plus 2-deoxyglucose and glycolytic lactate production was slowed by the 2-deoxyglucose. Acidification was slower with other substrates but generally tracked the respiration rates in Fig. 4B.
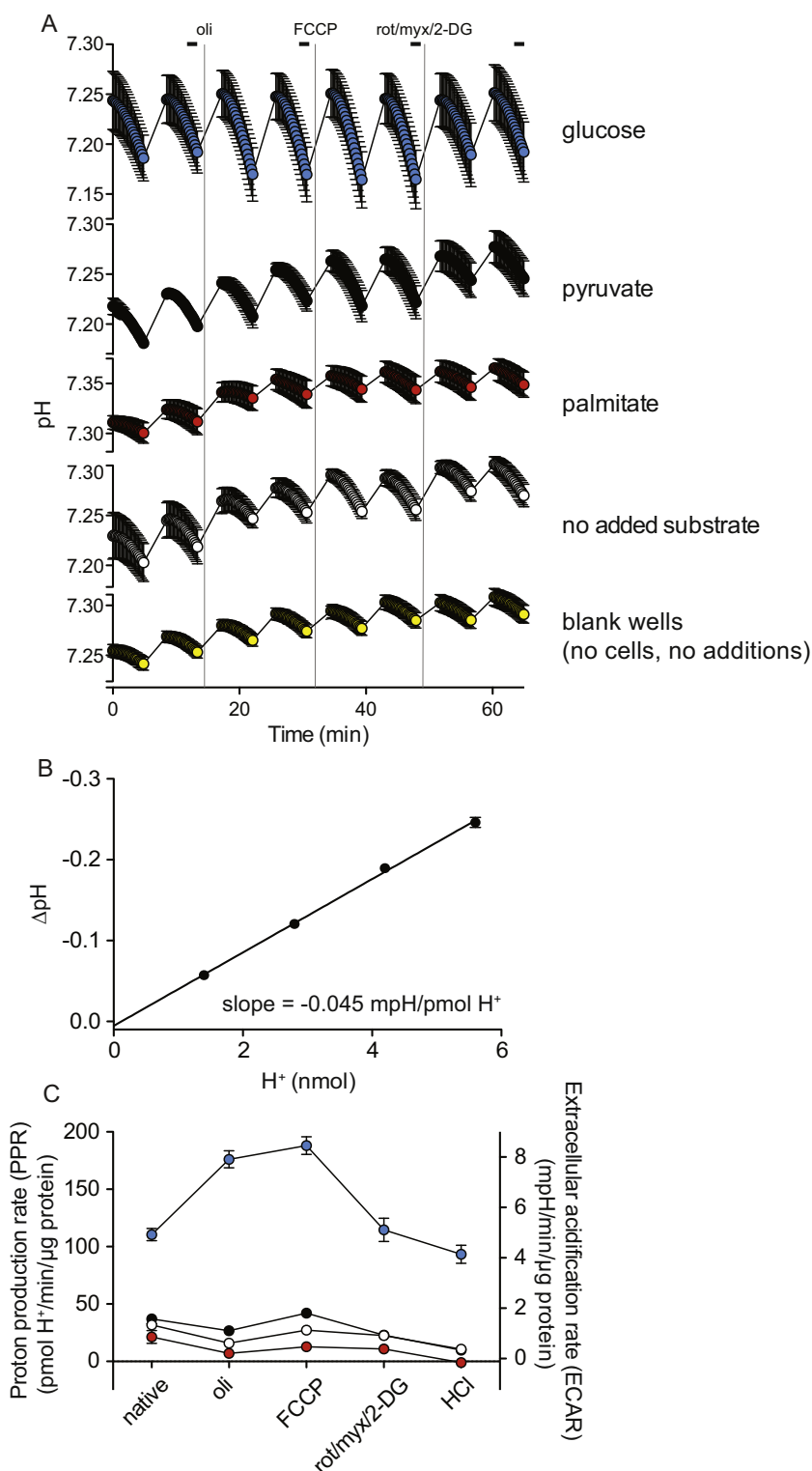
Fig. 5. Extracellular acidification and proton production rate. (A) Extracellular pH measured in the same experiment as Fig. 4B during measurement of cell respiratory control in C2C12 myoblasts using the Seahorse XF-24. Horizontal bars: data used for analysis of extracellular acidification rate. (B) Acid calibration in cell-free wells containing medium only (KRPH). Different amounts of HCl were added from the ports and the pH changes were assessed as in Fig. 2B, C. Values for HCl added in the 7 μL measuring volume. (C) Total extracellular acidification rate expressed as proton production rate (pmol H^+/min/μg protein, left axis) and as extracellular acidification rate (mpH/min/μg protein, right axis); data from (A) corrected where appropriate using the slope (buffering power) from (B), with rates in blank wells subtracted. Blue: glucose; black: pyruvate; no fill: no substrate; red: palmitate. All data are means ± SEM of $n = 8$ independent biological replicates.

Using the rotenone/myxothiazol-sensitive respiration data in Fig. 4B, we calculated the absolute rates of CO_2-derived acidification (see "theoretical considerations"). The absolute rates of proton production from CO_2 and lactate for each substrate in each phase of the cell respiratory control experiment of Fig. 4B are presented in Fig. 6A, calculated using Eq. (3).

We found that respiratory CO_2 contributed substantially to total extracellular acidification. In the presence of glucose under native
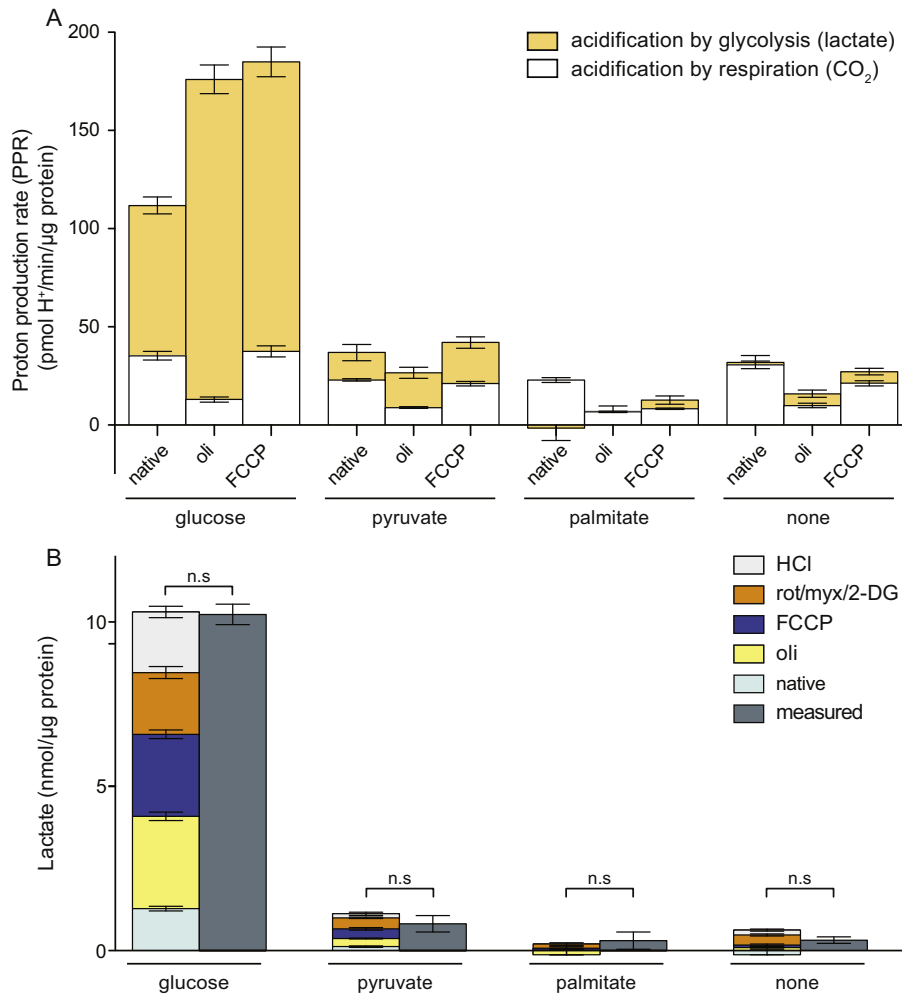
Fig. 6. Rates of extracellular acidification caused by glycolytic lactate production and respiratory CO_2 production by C2C12 myoblasts. (A) Contributions to extracellular proton production during the cell respiratory control experiments shown in Fig. 4B. Extracellular acidification caused by lactate production was calculated using Eq. (3) using the data in Figs. 5C and 4B and extracellular acidification caused by respiratory CO_2 was calculated from the data in Fig. 4B using the relationships in Materials and Methods. (B) Calculated and measured lactate production. Total lactate during the course of the experiment in Fig. 4B calculated from the sum of glycolytic acidification (pmol H^+/min/μg protein × min) at each stage of the assay in (A) assuming constant rates in each stage (stacked bars) compared to end point lactate measurement of the extracellular medium from the same samples (solid bars). Error values used in statistical analysis were calculated from the SEM of measured lactate and from propagated SEMs of predicted lactate. n.s.: $p > 0.05$, two-tailed paired Student's t-test. All data are means ± SEM of $n = 8$ independent biological replicates.

conditions, acidification was $34 \pm 2\%$ CO_2-derived, and only $66\% \pm 2\%$ lactate-derived. When mitochondrial ATP production was inhibited by oligomycin, respiratory CO_2 still accounted for $8 \pm 1\%$ of total proton production rate. The total extracellular acidification rate increased 1.6-fold after addition of oligomycin, but after correction for CO_2 production, the same data show that glycolytic lactate production increased 2.2-fold, illustrating the importance of making the correction. After addition of uncoupler, respiration and the acidification caused by respiratory CO_2 increased (and glycolytic rate decreased, perhaps because of intracellular acidification), increasing CO_2-derived acidification to $22\% \pm 2\%$. Thus, the proportion of extracellular acidification caused by respiratory CO_2 is not constant, but varies as expected with energy demand and the relative rates of glycolysis and the tricarboxylic acid cycle. Failure to correct for acidification caused by CO_2 production can have a large effect on the calculated fold-changes in glycolytic rate.

When pyruvate or palmitate was the added substrate, most of the extracellular acidification was caused by CO_2 production, as expected. Under native conditions $67\% \pm 7\%$ of the total measured proton production rate with pyruvate was from CO_2; for palmitate, this value was $113\% \pm 30\%$. In the absence of added substrate,

extracellular acidification was entirely accounted for by respiratory CO_2 ($102\% \pm 11\%$).

3.2.3. Lactate measurement verifies calculation of glycolytic extracellular acidification

In Fig. 6A, the rate of extracellular acidification caused by lactate production was calculated solely from the rates of respiration and proton production using Eq. (3). To verify this assessment, we measured the total lactate in the wells and compared it to the value predicted by glycolytic acidification, that is, the sum of lactate-derived proton production during each stage of the respiratory control experiment. The stacked bars in Fig. 6B show these predicted sums for each substrate. The final lactate measured was, within the error, equal to the predicted sum of lactate amounts, supporting the assumptions and calculations of glycolytic acidification rates using Eq. (3). In contrast, using the total acidification rates (i.e., uncorrected for respiratory acidification) for these calculations caused significant ($p \le 0.05$) overestimation of lactate production rates with all substrates except palmitate ($p = 0.08$) (not shown).
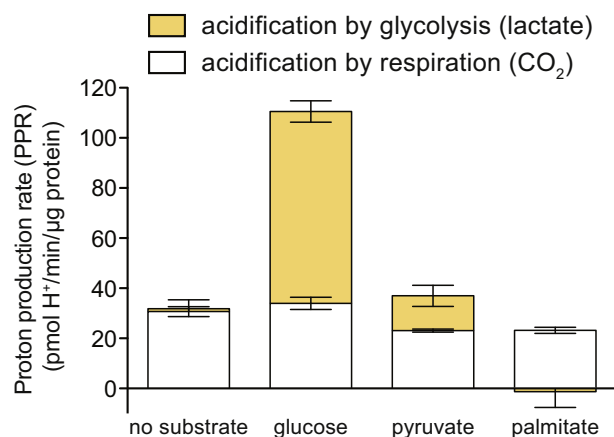
Fig. 7. Relative rates of proton production caused by glycolytic lactate production and respiratory CO_2 production by C2C12 myoblasts. Data extracted from Fig. 6 emphasize the important contributions of respiratory CO_2 production to total acidification rate in the native condition before addition of inhibitors.

3.2.4. Extracellular acidification caused by respiratory CO_2 in different cells under normal incubation conditions

Fig. 7 extracts the most important conclusions for native (i.e., no inhibitors) conditions from Fig. 6A, showing graphically that CO_2 production was a substantial contributor to the overall extracellular acidification rate in the presence of glucose and dominated the rate in all other conditions. Crucially, if CO_2-dependent acidification is not accounted for, the change in "glycolytic rate" on introduction of glucose to cells would be calculated as 3.5-fold, but after correction, it is clear that the real change is orders of magnitude greater.

To determine the general importance of CO_2-dependent acidification, we measured it in other cell lines under native conditions (Table 1). For cancer cell lines, the respiratory acidification rate varied from small (SJSA-1) to a substantial proportion of the total (MCF7). The I6 human embryonic stem cells and derived neural stem cells showed primarily respiratory acidification. Whole neurons and isolated synaptosomes showed primarily glycolytic acidification. Finally, both INS1E insulinoma cells (which lack lactate dehydrogenase) and dispersed rat islets showed entirely respiratory acidification.

We also used Eq. (3) to analyse published data collected using the Seahorse platform. Table 2 shows that CO_2 production generates a substantial proportion of the total extracellular acidification in most cell types. The contribution varied, with values ranging from 0% to 100%, independent of absolute acidification rate. These results demonstrate the

vital importance of our correction to the interpretation of extracellular acidification. Eq. (3) provides a straightforward means to correct experimental data in this way.

4. Discussion

We demonstrate here the substantial contribution that respiratory CO_2 can make to extracellular acidification. Previous estimates based on oxamate inhibition of lactate dehydrogenase in cultured cancer cells given glucose suggested that the contribution of respiration was less than 20% and could be neglected [8]. However, CO_2 has previously been reported to be a considerable acidification source in solid tumours [7,42]. We also show that extracellular acidification is the sum of respiratory acidification and glycolytic proton production measured by lactate assay, confirming no major additional acidification mechanisms in the conditions we have studied.

The contribution from each source to total acidification differs according to cell type, substrates used, and by the limitations placed on respiration. To measure the glycolytic lactate production rate separately from respiration, it is therefore essential in either the experimental design or post-hoc data analysis to measure and subtract CO_2-derived proton production. This is particularly true for relative comparisons; without knowing the acidification sources, it is impossible to be sure whether any change in extracellular acidification is caused by a change in glycolytic or respiration rate. However, with correction, it is possible to determine both the source and quantity of acidification rate changes.

We describe a simple method to make this correction using Eq. (3) and measurements of the rates of extracellular acidification and mitochondrial oxygen consumption. The only other information required is the pH, the buffering power of the solution (to convert pH changes to rates of proton production, PPR) and estimates of RQ and the net H^+/CO_2 ratio for the substrate being oxidized (for calculation of max H^+/O_2). The buffering power of the solution can be measured at the end of the experiment by adding known amounts of HCl (Figs. 2 and 5), measured in bulk in a separate experiment (Tables 1 and 2), or imported from other sources. Correct calculation of PPR within the Seahorse software requires the entry of the buffering power of the medium before the experiment. The max H^+/O_2 ratios for complete oxidation of different substrates are known or can be readily calculated (see Materials and Methods). If a significant proportion of the substrate is not completely oxidised, correction will require estimation of the appropriate overall reactions. For example, during rapid cell growth, reducing equivalent is diverted from oxygen to biosynthesis, so OCR will underestimate respiratory acidification and glycolysis will be overestimated if normal max H^+/O_2 values are used; or if added

Table 1

Contribution of CO_2-dependent acidification to total extracellular acidification in different cells. Respiratory PPR was calculated from the rotenone/myxothiazol-sensitive OCR as described in Materials and Methods using data from Seahorse output files. The buffering power of the relevant medium was measured using a pH meter to record the pH changes in response to known additions of HCl. Max H^+/O_2 was assumed to be 1 for all calculations; error in this assumption will affect the respiratory PPR values: if only pyruvate was oxidized values should be multiplied by 0.8; if only glutamine was oxidized they should be multiplied by 0.67. The absence of added carbonic anhydrase could cause overestimation of CO_2-dependent acidification. Data are means ± SEM of n independent experiments (SEM of 4 technical replicates for ZR75-30 cells and dispersed rat islets, and 16 technical replicates for INS1E cells). PPR, proton production rate; min TES, minimal TES buffer (see Materials and Methods).

Cells	Added substrate	Respiratory PPR (% of total PPR)	n	Assay medium	Buffering power ($-$mpH/pmol H^+)
Cancer cells					
MCF7	Glucose	76 ± 10	3	min TES	0.01
MCF7 (State IV)	Glucose + oligomycin	10 ± 1	3	min TES	0.01
ZR75-30	Glucose	38 ± 6	1	min TES	0.01
ZR75-1	Glucose	23 ± 4	3	min TES	0.01
SJSA-1	Glucose	9 ± 1	3	min TES	0.01
Cell lines and primary cells					
Dispersed rat islets	Glucose/glutamine	96 ± 7	1	RPMI	0.01
INS1E	Glucose/glutamine	93 ± 7	1	min TES	0.01
I6 embryonic stem cells [18]	Glucose/pyruvate/glutamine	57 ± 6	3	XF DMEM	0.1
I6 neuronal stem cells [18]	Glucose/pyruvate/glutamine	42 ± 10	3	XF DMEM	0.1
Rat primary cortical neurons	Glucose/pyruvate	16 ± 6	5	min TES	0.01
Cortical synaptosomes [22]	Glucose/pyruvate	9 ± 3	5	min TES	0.01

Table 2

Contribution of CO_2-dependent acidification to total extracellular acidification under basal conditions calculated from published data. Glucose was added in all cases except where noted in [39]; amino acids were added in some cases. MCF10A variants: −T1K: pre-neoplastic; −CA1h: low-grade tumorigenic; −CA1a: high-grade tumorigenic [29]. Respiratory PPR was calculated as described in Materials and Methods, with max H^+/O_2 assumed to be 1 (error in this assumption will affect the respiratory PPR values: if only pyruvate was oxidized values should be multiplied by 0.8; if only glutamine was oxidized they should be multiplied by 0.67). The buffering power of the relevant medium was measured using a pH meter to record the pH changes in response to known additions of HCl. The absence of added carbonic anhydrase could cause overestimation of CO_2-dependent acidification. Respiratory PPR was independent of total PPR ($r^2 = 0.001$). *Values assumed to have been normalized to protein. °Values normalized to cell number. Values are means ± SEM of 3–5 experiments.

Cells	Respiratory PPR (% of total PPR)	Total PPR (pmol H^+/min/µg protein)	Source of data
Cell lines			
MCF10A-T1K	73 ± 4	8000 ± 640*	[29]
MCF10A	71 ± 36	22500 ± 2900*	[30,29]
hFOB	47 ± 2	6000 ± 160	[31]
mESC Htt 140/7	36 ± 0	500 ± 0	[32]
mESC Htt 7/7	21 ± 0	500 ± 0	[32]
mESC Htt −/−	5 ± 1	800 ± 50	[32]
Cancer cells			
MCF10CA1h	131 ± 39	4000 ± 230*	[29]
BT-474	95 ± 7	20000 ± 3500	[30]
Saos2	63 ± 0	3500 ± 143	[31]
Rhabdomyosarcoma	57 ± 6	500 ± 64	[33]
LL/2	53 ± 11	2000 ± 280	[34]
HOS	51 ± 1	5700 ± 512	[31]
MCF10CA1a	51 ± 13	7500 ± 290*	[29]
MLE-15	48 ± 10	25 ± 5*	[35]
BCAP 37	32 ± 4	400 ± 30	[36]
4 T1	20 ± 4	250 ± 21	[36,37]
HCT116	20 ± 2	3000 ± 190	[34]
B16F10	23 ± 2	3250 ± 110	[34]
HeLa	20 ± 2	470 ± 23	[36]
SW480	14 ± 0	580 ± 10	[38]
A549	12 ± 1	800 ± 51	[36]
MDA-MB-231	8 ± 2	52125 ± 13300	[30,34]
PC3m	9 ± 2	4500 ± 530	[34]
LM7	5 ± 1	12500 ± 952	[31]
143B	4 ± 1	17000 ± 3000	[31]
Primary cells			
CD8 + T cells effector [pyruvate/glutamine]	96 ± 26	400 ± 80	[39]
Monocytes	91 ± 2	100 ± 5°	[40]
PBMC (mixed)	66 ± 2	80 ± 2°	[40]
T cells	55 ± 8	35 ± 5°	[40]
AT-II primary	46 ± 5	50 ± 5*	[35]
Rat primary striatal neurons	42 ± 6	567 ± 83	[41]
CD8 + T cells naïve [glucose]	31 ± 1	150 ± 4	[39]
CD8 + T cells naïve [pyruvate/glutamine]	30 ± 1	100 ± 4	[39]
CD8 + T cells effector [glucose]	21 ± 9	800 ± 240	[39]
Neutrophils	3 ± 1	230 ± 28°	[40]

pyruvate is converted to glycogen or dismutated to lactate and CO_2, OCR will overestimate respiratory acidification and glycolysis will be underestimated if normal max H^+/O_2 values are used. In all cases, we recommend adding exogenous carbonic anhydrase to ensure quantitative conversion of CO_2 to $HCO_3^- + H^+$ and avoid ambiguity. Finally, glycolytic rate as calculated using Eq. (3) can be verified by end point lactate measurement if there is uncertainty about the substrates being utilized or if the assay configuration might allow CO_2 to be lost from the assay.

Once the absolute rates of both mitochondrial respiration and glycolysis are known, the rates of ATP production from each pathway can be estimated [18]. The proportions of glucose and glycogen consumption must be known or assumed. The total rate of glycolytic ATP production is the sum of the rates from glycolysis to lactate and glycolysis to pyruvate that subsequently enters the tricarboxylic acid cycle.

In both cases, glycolysis from glucose yields 1 ATP per pyruvate or lactate formed, so the total rate of glycolytic ATP formation can be calculated directly from the lactate-derived proton production plus the 0.33 ATP/O_2 formed during generation of pyruvate destined for oxidation (calculated from the rotenone-sensitive oxygen consumption rate). For glycolysis from glycogen, the yields are 1.5 ATP/lactate and 0.5 ATP/O_2.

The yield of ATP from oxidative phosphorylation can be calculated from the oxygen consumption rate driving ATP synthesis, which is estimated from the decrease in respiration rate when oligomycin is added—the correction for compensatory changes in proton leak following oligomycin addition is ∼10% [43]. Multiplication of the oligomycin-sensitive respiration rate by the appropriate P/O ratio (ATP formed/[O] consumed) gives the rate of ATP synthesis by oxidative phosphorylation. P/O ratios are discussed in [44]. The maximum value for complete oxidation of pyruvate derived from glucose (excluding glycolytic ATP and assuming 2.67 H^+/ATP at the ATP synthase [45]) is 2.63 (31.5 ATP per glucose, not 38 as commonly asserted in textbooks). For complete oxidation of palmitate the value is 2.5 (113 ATP per palmitate, not 129).

To apply these findings, a user would perform a standard respiratory control assay, measuring both OCR and ECAR (e.g., [5]). The only additional requirement is determination of the buffering power of the assay medium, which may be measured by injections of standard acid separately or during the experiment. In the Seahorse platform, it can be entered into the software during experimental setup and total PPR may be read directly from the software output. Alternatively, buffering power may be incorporated post hoc into data analysis calculations to determine total PPR from the output ECAR values. In our hands, these approaches yield the same results. Note that the total pH change should be less than ∼0.2 pH units to maintain reasonable linearity of the buffering power approximations. The corrected glycolytic rate, PPR_{glyc}, is then determined from PPR_{tot} using Eq. (3). This requires a value for max H^+/O_2. If the substrate used by the cells is known or safely estimated, max H^+/O_2 is readily calculated. If it is not, the values for the usual substrates vary only from 0.65 to 1.0 (see Materials and Methods), so using a value of 1 or an intermediate value will still allow qualitative work. The values of PPR_{glyc} and PPR_{resp} can be used to calculate the oxidative and glycolytic sources of ATP production as described above.

5. Conclusion

Correction for the contribution of respiratory CO_2 to extracellular acidification rate as described here should greatly improve assessments of glycolytic rate under different conditions and allow more reliable conclusions about the magnitude of fold-changes and the regulation of glycolytic rate in a variety of different cells and contexts.

Author contributions

MDB and DGN conceived the investigation. SAM and MDB designed the experiments and wrote the manuscript. RLG and AAG designed and carried out some experiments in Table 1; SAM carried out all other experiments. All authors reviewed the manuscript.

Acknowledgements

References

[1] S. Nadanaciva, P. Rana, G.C. Beeson, D. Chen, D.A. Ferrick, C.C. Beeson, Y. Will, Assessment of drug-induced mitochondrial dysfunction via altered cellular respiration and acidification measured in a 96-well platform, J. Bioenerg. Biomembr. 44 (2012) 421–437.

[2] D.G. Nicholls, V.M. Darley-Usmar, M. Wu, P.B. Jensen, G.W. Rogers, D.A. Ferrick, Bioenergetic profile experiment using C2C12 myoblast cells, J. Vis. Exp. 46 (2010) 2511.

[3] C. Diepart, J. Verrax, P.B. Calderon, O. Feron, B.F. Jordan, B. Gallez, Comparison of methods for measuring oxygen consumption in tumor cells in vitro, Anal. Biochem. 396 (2010) 250–256.

[4] A.A. Gerencser, A. Neilson, S.W. Choi, U. Edman, N. Yadava, R.J. Oh, D.A. Ferrick, D.G. Nicholls, M.D. Brand, Quantitative microplate-based respirometry with correction for oxygen diffusion, Anal. Chem. 81 (2009) 6868–6878.

[5] M.D. Brand, D.G. Nicholls, Assessing mitochondrial dysfunction in cells, Biochem. J. 435 (2011) 297–312.

[6] M.D. Brand, The proton leak across the mitochondrial inner membrane, Biochim. Biophys. Acta 1018 (1990) 128–133.

[7] E. Hütter, K. Renner, P. Jansen-Dürr, E. Gnaiger, Biphasic oxygen kinetics of cellular respiration and linear oxygen dependence of antimycin A inhibited oxygen consumption, Mol. Biol. Rep. 29 (2002) 83–87.

[8] M. Wu, A. Neilson, A.L. Swift, R. Moran, J. Tamagnine, D. Parslow, S. Armistead, K. Lemire, J. Orrell, J. Teich, S. Chomicz, D.A. Ferrick, Multiparameter metabolic analysis reveals a close link between attenuated mitochondrial bioenergetic function and enhanced glycolysis dependency in human tumor cells, Am. J. Physiol. 292 (2006) C125–C136.

[9] G.N. Shah, Y. Morofuji, W.A. Banks, T.O. Price, High glucose-induced mitochondrial respiration and reactive oxygen species in mouse cerebral pericytes is reversed by pharmacological inhibition of mitochondrial carbonic anhydrases: implications for cerebral microvascular disease in diabetes, Biochem. Biophys. Res. Commun. 440 (2013) 354–358.

[10] U. Dier, D.-H. Shin, L.P.M.P. Hemachandra, L.M. Uusitalo, N. Hempel, Bioenergetic analysis of ovarian Cancer cell lines: profiling of histological subtypes and identification of a mitochondria-defective cell line, PLoS One 9 (2014) e98479.

[11] G.A. Benavides, Q. Liang, M. Dodson, V. Darley-Usmar, J. Zhang, Inhibition of autophagy and glycolysis by nitric oxide during hypoxia–reoxygenation impairs cellular bioenergetics and promotes cell death in primary neurons, Free Radic. Biol. Med. 65 (2013) 1215–1228.

[12] C. Affourtit, C.L. Quinlan, M.D. Brand, Measurement of proton leak and electron leak in isolated mitochondria, Methods Mol. Biol. 810 (2011) 165–182.

[13] G.W. Rogers, M.D. Brand, S. Petrosyan, D. Ashok, A.A. Elorza, D.A. Ferrick, A.N. Murphy, High throughput microplate respiratory measurements using minimal quantities of isolated mitochondria, PLoS One 6 (2011) e21746.

[14] H. Blau, C. Chiu, C. Webster, Cytoplasmic activation of human nuclear genes in human heterocaryons, Cell 32 (1983) 1171–1180.

[15] J. Bartek, R. Iggo, J. Gannon, D. Lane, Genetic and immunochemical analysis of mutant p53 in human breast cancer lines, Oncogene 5 (1990) 893–899.

[16] W. Roberts, E. Douglass, S. Peiper, Amplification of the gli gene in childhood sarcomas, Cancer Res. 49 (1989) 5407–5413.

[17] H.D. Soule, T.M. Maloney, S.R. Wolman, W.D.J. Peterson, R. Brenz, C.M. McGrath, J. Russo, R.J. Pauley, R.F. Jones, S.C. Brooks, Isolation and characterization of a spontaneously immortalized human breast epithelial cell line, MCF-10, Cancer Res. 50 (1990) 6075–6086.

[18] M.J. Birket, A.L. Orr, A.A. Gerencser, D.T. Madden, C. Vitelli, A. Swistowski, M.D. Brand, X. Zeng, A reduction in ATP demand and mitochondrial activity with neural differentiation of human embryonic stem cells, J. Cell Sci. 124 (2011) 348–358.

[19] C. Chinopoulos, A.A. Gerencser, M. Mandi, K. Mathe, B. Törőcsik, J. Doczi, L. Turiak, G. Kiss, C. Konràd, S. Vajda, V. Vereczki, R. Oh, V. Adam-Vizi, Forward operation of adenine nucleotide translocase during F0F1-ATPase reversal: critical role of matrix substrate-level phosphorylation, FASEB J. 24 (2010) 2405–2416.

[20] G.L. Szot, P. Koudria, J.A. Bluestone, Murine pancreatic islet isolation, J. Vis. Exp. 7 (2007) 255.

[21] M. Asfari, D. Janjic, P. Meda, G. Li, P.A. Halban, C.B. Wollheim, Establishment of 2-mercaptoethanol-dependent differentiated insulin-secreting cell lines, Endocrinology 130 (1992) 167–178.

[22] S.W. Choi, A.A. Gerencser, D.G. Nicholls, Bioenergetic analysis of isolated cerebrocortical nerve terminals on a microgram scale: spare respiratory capacity and stochastic mitochondrial failure, J. Neurochem. 109 (2009) 1179–1191.

[23] R.H. Garrett, C.M. Grisham, Biochemistry, Cengage Learning, Boston, MA, 2012.

[24] A.P. Halestrap, N. Price, The proton-linked monocarboxylate transporter (MCT) family: structure, function and regulation, Biochem. J. 343 (1999) 281–299.

[25] A. Bonen, J.J. Luiken, S. Liu, D.J. Dyck, B. Kiens, S. Kristiansen, L.P. Turcotte, G.J. Van Der Vusse, J.F. Glatz, Palmitate transport and fatty acid transporters in red and white muscles, Am. J. Physiol. 275 (1998) E471–E478.

[26] W. Dott, P. Mistry, J. Wright, K. Cain, K.E. Herbert, Modulation of mitochondrial bioenergetics in a skeletal muscle cell line model of mitochondrial toxicity, Redox Biol. 2 (2014) 224–233.

[27] J. Patková, M. Anděl, J. Trnka, Palmitate-induced cell death and mitochondrial respiratory dysfunction in myoblasts are not prevented by mitochondria-targeted antioxidants, Cell. Physiol. Biochem. 33 (2014) 1439–1451.

[28] M. Elkalaf, M. Anděl, J. Trnka, Low glucose but not galactose enhances oxidative mitochondrial metabolism in C2C12 myoblasts and myotubes, PLoS One 8 (2013) (e70772-e70772).

[29] P.G. Shaw, R. Chaerkady, T. Wang, S. Vasilatos, Y. Huang, B. Van Houten, A. Pandey, N.E. Davidson, Integrated proteomic and metabolic analysis of breast cancer progression, PLoS One 8 (2013) e76220.

[30] M. Mouradian, K.D. Kikawa, B.P. Dranka, S.M. Komas, B. Kalyanaraman, R.S. Pardini, Docosahexaenoic acid attenuates breast cancer cell metabolism and the Warburg phenotype by targeting bioenergetic function, Mol. Carcinog. (2014), http://dx.doi.org/10.1002/mc.22151 (epub ahead of print).

[31] A.H. Giang, T. Raymond, P. Brookes, K. de Mesy Bentley, E. Schwarz, R. O'Keefe, R. Eliseev, Mitochondrial dysfunction and permeability transition in osteosarcoma cells showing the Warburg effect, J. Biol. Chem. 288 (2013) 33303–33311.

[32] I. Ismailoglu, Q. Chen, M. Popowski, L. Yang, S.S. Gross, A.H. Brivanlou, Huntingtin protein is essential for mitochondrial metabolism, bioenergetics and structure in murine embryonic stem cells, Dev. Biol. 391 (2014) 230–240.

[33] R.A. Vaughan, R. Garcia-Smith, M.A. Barberena, M. Bisoffi, K. Trujillo, C.A. Conn, Treatment of human muscle cells with popular dietary supplements increase mitochondrial function and metabolic rate, Nutr. Metab. (Lond) 9 (2012) 101.

[34] K.M. Bailey, J.W. Wojtkowiak, H.H. Cornnell, M.C. Ribeiro, Y. Balagurunathan, A.I. Hashim, R.J. Gillies, Mechanisms of buffer therapy resistance, Neoplasia 16 (2014) (354–364.e353).

[35] R.G. Lottes, D.A. Newton, D.D. Spyropoulos, J.E. Baatz, Alveolar type II cells maintain bioenergetic homeostasis in hypoxia through metabolic and molecular adaptation, Am. J. Phys. 306 (2014) L947–L955.

[36] J. Xie, H. Wu, C. Dai, Q. Pan, Z. Ding, D. Hu, B. Ji, Y. Luo, X. Hu, Beyond Warburg effect – dual metabolic nature of cancer cells, Sci. Rep. 4 (2014) 4927.

[37] A. Rizwan, I. Serganova, R. Khanin, H. Karabeber, X. Ni, S. Thakur, K.L. Zakian, R. Blasberg, J.A. Koutcher, Relationships between LDH-A, lactate, and metastases in 4 T1 breast tumors, Clin. Cancer Res. 19 (2013) 5158–5169.

[38] K.T. Pate, C. Stringari, S. Sprowl-Tanio, K. Wang, T. TeSlaa, N.P. Hoverter, M.M. McQuade, C. Garner, M.A. Digman, M.A. Teitell, R.A. Edwards, E. Gratton, M.L. Waterman, Wnt signaling directs a metabolic program of glycolysis and angiogenesis in colon cancer, EMBO J. 33 (2014) 1454–1473.

[39] M. Sukumar, J. Liu, Y. Ji, M. Subramanian, J.G. Crompton, Z. Yu, R. Roychoudhuri, D.C. Palmer, P. Muranski, E.D. Karoly, R.P. Mohney, C.A. Klebanoff, A. Lal, T. Finkel, N.P. Restifo, L. Gattinoni, Inhibiting glycolytic metabolism enhances CD8+ T cell memory and antitumor function, J. Clin. Invest. 123 (2013) 4479–4488.

[40] M. Pelletier, L.K. Billingham, M. Ramaswamy, R.M. Siegel, Extracellular Flux Analysis to Monitor Glycolytic Rates and Mitochondrial Oxygen Consumption, Methods Enzymol. 542 (2014) 125–149.

[41] C. Gouarné, G. Tardif, J. Tracz, V. Latyszenok, M. Michaud, L.E. Clemens, L. Yu-Taeger, H.P. Nguyen, T. Bordet, R.M. Pruss, Early deficits in glycolysis are specific to striatal neurons from a rat model of Huntington Disease, PLoS One 8 (2013) e81528.

[42] G. Helmlinger, A. Sckell, M. Dellian, N.S. Forbes, R.K. Jain, Acid production in glycolysis-impaired tumors provides new insights into tumor metabolism, Clin. Cancer Res. 8 (2002) 1284–1291.

[43] C. Affourtit, M.D. Brand, Measuring mitochondrial bioenergetics in INS-1E insulinoma cells, Methods Enzymol. 457 (2009) 405–424.

[44] M.D. Brand, The efficiency and plasticity of mitochondrial energy transduction, Biochem. Soc. Trans. 33 (2005) 897–904.

[45] I.N. Watt, M.G. Montgomery, M.J. Runswick, A.G. Leslie, J.E. Walker, Bioenergetic cost of making an adenosine triphosphate molecule in animal mitochondria, Proc. Natl. Acad. Sci. U. S. A. 107 (2010) 16823–16827.